Debonding detection in CFRP reinforced concrete structure using guided waves

Paritosh Giri[1], Sergey Kharkovsky[2], Xinqun Zhu[3], Simon Martin Clark[4] and Bijan Samali[2]

[1]Department of Physics and Astronomy, Macquarie University, Sydney, NSW, Australia

[2]Centre for Infrastructure Engineering, School of Computing, Engineering and Mathematics, Western Sydney University, Penrith, NSW, Australia

[3]School of Civil and Environmental Engineering, University of Technology Sydney, Ultimo, NSW, Australia

[4]Department of Earth and Planetary Sciences, Macquarie University, Sydney, NSW, Australia

Abstract

Guided waves are conventionally used in different non-destructive testing applications because of their cost-effectiveness and light-weight transducers that are easy to incorporate into the structure. The non-destructive evaluation of interfacial defects such as debonding in the composite structure is critical for the safety and long-term use. This paper presents a guided wave technique to detect a variety of debondings in carbon fibre reinforced concrete structure. Five composite specimens were prepared with different debondings: lengthwise, widthwise and patch debonding at different positions of the specimen with respect to the transducers. The guided wave received by the signal at a perfect bonding is taken as a reference. This signal is compared with the received signal at the different debonding conditions. The quantification of the debonding was performed using three damage indices: correlation coefficient, change in P2P and root mean square deviation. The results confirmed that the damage indices correlate linearly with the extent of the debonding which can be used to predict the debond conditions. This method is effective in the non-destructive detection of interfacial defects in an existing structure without special preparation.

Keywords: guided waves, piezoelectric sensing, debonding, composite structure, CFRP reinforcement, structural health monitoring, non-destructive evaluation.

1. Introduction

Carbon fibre reinforced polymers (CFRPs) are gaining popularity in the construction industry, mainly, to strengthen structural members, to provide additional durability to the structures and

to repair the aging structures [1, 2]. Civil infrastructures such as bridges deteriorate due to several factors such as corrosion, excessive load or change in operating conditions. CFRP composites being light weight and having high resistance to corrosion is a suitable candidate for their reinforcement. CFRP plates or laminates are either externally bonded to a concrete surface of the structure, used as an external tube for concrete filling also called as a concrete-filled FRP tube (CFFT) or used to wrap concrete beams which are also called as concrete jacketing [3-5]. The bond between the CFRP and the concrete member is critical in maintaining the effectiveness of the strengthening system [6, 7]. However, the poor construction quality, aging, shrinkage of concrete, and deterioration due to moisture may cause debonding between CFRP and concrete surfaces [8]. These debonding should be detected at an early stage to ensure the structural integrity and safety of these composite structures.

Several techniques have been reported to detect debonding between CFRP composites and concrete. A microwave imaging technique based on near-field approach was applied to detect debonding between CFRP laminates and concrete using two-dimensional images of the structure under test [9, 10]. Infrared thermography was used to monitor air-filled debonds in fibre reinforced polymer (FRP) strengthened RC bridge decks [11], and CFRP strengthened concrete beam composites [12]. Acoustic emission monitoring technique was applied to detect debonds in concrete slab specimens strengthened with CFRP strips using parametric analysis, intensity analysis and principal component analysis method [13]. Acoustic-laser technique was used to detect interfacial defects in CFRP bonded concrete structure which used acoustic excitation to vibrate the target and a laser beam to characterise the vibration behaviour [14]. An impact-echo method was applied to detect debonding flaws at the epoxy-concrete interfaces in near-surface mounted CFRP strengthening beams [15]. A far-field radar technique was utilised by combining synthetic aperture radar measurements with the back projection algorithms to detect interfacial defects in FRP wrapped concrete structure [16].

Lamb wave techniques are conventionally used in different non-destructive testing applications [17, 18]. Lamb waves are the types of ultrasonic guided waves which are sensitive to small damage and have a capability of large area scanning with a small number of transducers. Besides, the piezoelectric transducers used to generate lamb waves are light-weight, economical and easy to incorporate into the structure [19]. Lamb waves are commonly used to detect fatigue cracks and debonds in metallic and composite structures [20]. Built-in piezoelectric discs were utilised to detect debonding between reinforced concrete and steel

rebar [21]. A surface mounted PZT was used as an actuator and an embedded PZT as a sensor to detect interfacial debonding between steel tube and a concrete core in a composite structure [22]. An electro-mechanical impedance based model was developed which utilised infinitesimal-length springs to model the bond between a metal plate and a composite patch and ultimately detect the debond condition [23]. Guided wave propagation and spectral element method were used to detect interfacial defects between the embedded steel rebar and a reinforced concrete structure [24]. In this technique, the spectral model was developed, and a numerical simulation was carried out which was verified using experimental measurements [25]. The lamb wave techniques described above to detect interfacial defects utilised embedded PZTs inside the structure which cannot be applied in an existing structure and requires special preparation of the structure. An electro-mechanical impedance-based technique using surface mounted PZT ceramic patches was utilised to detect debond between a concrete beam and a CFRP laminate [26]. Similarly, the statistical analysis method was used on the received lamb wave signal to detect interfacial defects in concrete-steel interface [27]. Another, statistical analysis method based on lamb wave detected gaps between the CFRP plate and concrete structure and predicted the shrinkage of concrete inside the reinforced CFRP plate [28].

As mentioned previously, most of the lamb wave techniques need the transducers to be embedded inside the structure while the surface mounted transducer techniques are still under development and have not shown the capability of detecting a wide range of debondings. This study aims to address this research gap by developing a surface mounted piezoelectric sensing technique capable of detecting extensive debonding damages along different locations in the composite structure. For this purpose, three different damage indices are used to detect and quantify the debondings. These damage indices are applied to the received lamb wave signal before and after the damage. The experimental results show that the method is effective in detecting different debondings with all the indices correlating with the extent of the damage. The proposed technique is entirely non-destructive, economical and needs minimal signal processing.

2. Measurement approach and specimens

The measurement system consisted of two piezoelectric transducers (PZTs), signal generation and data acquisition unit and a computer as shown in Figure 1. Each PZT disc had a diameter of 6.35 mm and a resonant frequency of 300 kHz in a radial mode. These transducers were

attached to the external surface of the CFRP plate at a distance of 50 mm from each other. One piezoelectric transducer was used as an actuator (A1) while the other was used as a sensor (S1). Both piezoelectric transducers were connected to a signal generation and data acquisition unit. A computer was connected to the signal generation and data acquisition unit which was used to relay command for signal generation and data acquisition.

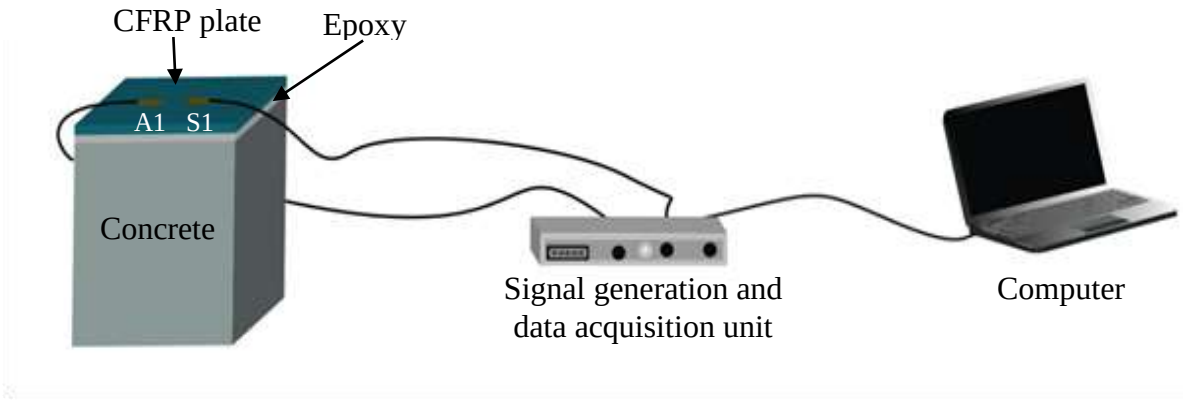

Figure 1. Schematic of the experimental setup of a piezoelectric sensing system for debond detection.

A sine burst signal with 5 peaks was used as an actuation signal. This signal had a peak-to-peak amplitude of 16 V as shown in Figure 2(a). The frequency sweeps from 100 kHz to 500 kHz at a step size of 100 kHz was performed to determine a suitable excitation frequency. The received signal had the highest amplitude at a frequency of 300 kHz which also matched the resonant frequency of the piezoelectric transducer. Thus, this frequency was used as an excitation frequency. The generated wave propagated along the CFRP plate and received by the sensor when the structure was intact (reference) and at various debonds between CFRP plate and concrete as shown in Figure 2(b). The sampling rate of 48 MS/s was used for data acquisition, and the gain of 40 dB was applied to the signal received by the sensor. This signal was then sent to the computer where the data was saved for comparison and statistical analysis. The changes in the received signal were used to determine the presence of debonding between the CFRP plate and concrete.

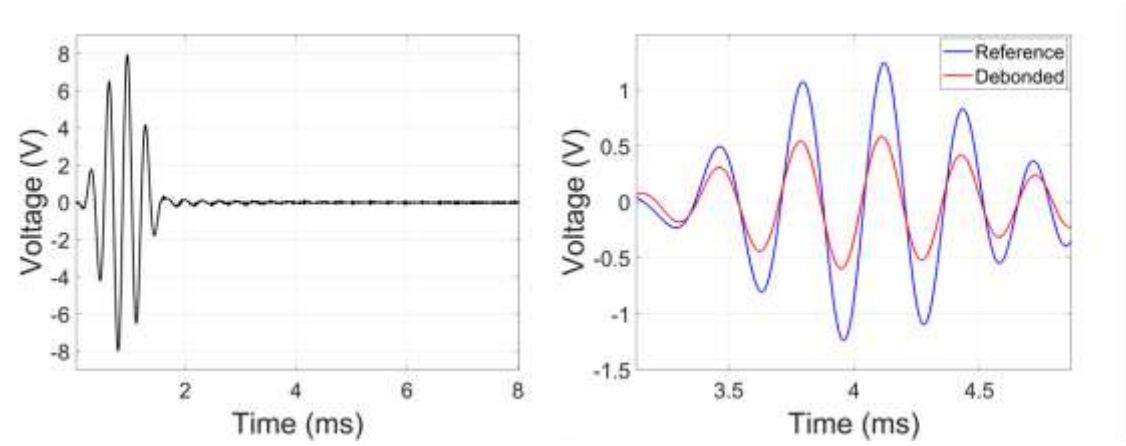

(a) (b)

Figure 2. (a) Actuation signal and (b) sensor signal showing the amplitude difference between the reference and debonded signal.

Multiple measurements were taken when the structure was intact (i.e. without debonding) and the average of these measurements was taken as a reference. Then, multiple measurements were taken at different types and sizes of debondings between CFRP plate and concrete. Side debondings in the structure were created by scraping out the epoxy layer from the sides of the composite structure using an electric cutter while the debondings at the middle of the composite structure were created while applying the epoxy layer to the concrete. The experimental setup for the measurement is shown in Figure 3.

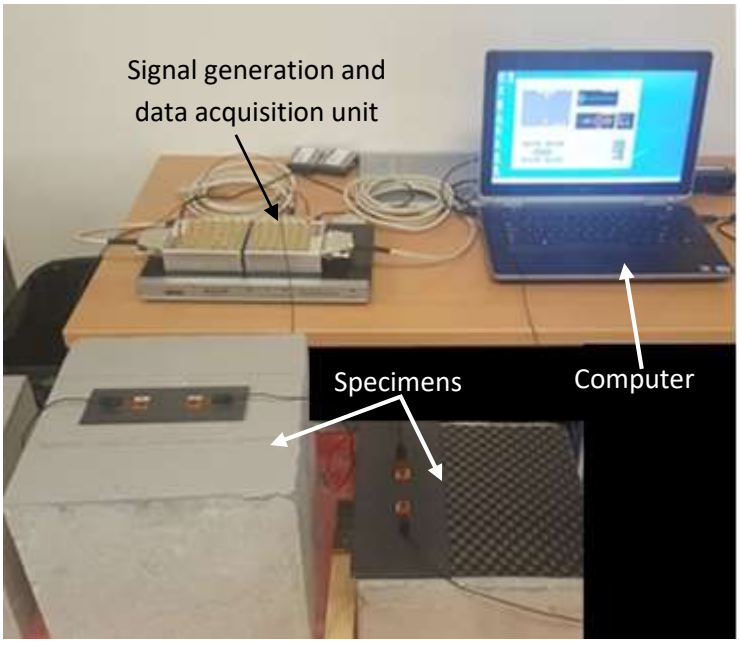

Figure 3. Experimental setup.

Several specimens were prepared with a variety of debondings such as lengthwise, widthwise and patch debondings in the structure which will be explained in the next section. The specimens included a concrete cube with a dimension of 250 mm x 250 mm x 250 mm. The concrete cube was prepared by mixing cement, sand and coarse aggregates at a ratio of 1:2:3. Five different sizes of CFRP plates were used for the investigation: 240 mm x 100 mm x 5 mm (referred to as specimen 1), 150 mm x 50 mm x 2 mm (referred to as specimen 2), 235 mm x 155 mm x 2 mm (referred to as specimen 3), 150 mm x 50 mm x 2 mm (referred to as specimen 4) and 190 mm x 100 mm x 5 mm (referred to as specimen 5). These CFRP plates were bonded to the concrete cubes using an epoxy Sikadur-30. Sikadur-30 is an adhesive mortar based on 2-component solvent free epoxy resin which is used to bond structural reinforcements to other substrates [29]. Sikadur-30 was mixed in the laboratory by combining the Part A (Resin) and Part B (Hardener) in the ratio of 3:1. Before mixing, these components were thoroughly stirred using a slow running stirrer. Then, Part B was decanted into Part A and mixed thoroughly until a uniform colour was achieved. Once a streaky colour was obtained, the epoxy was applied immediately to the cleaned and abraded concrete surface.

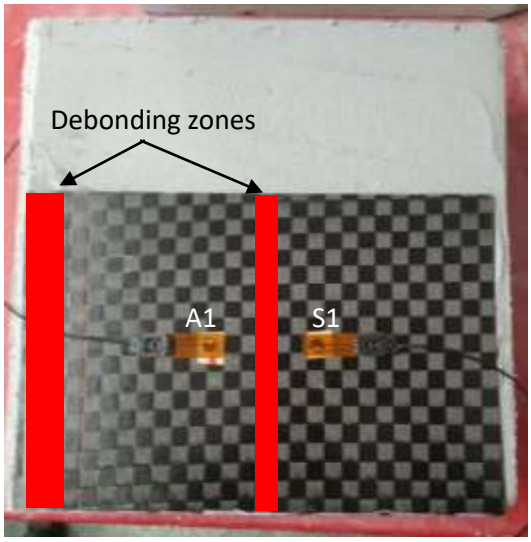

Figure 4. Photographic image of the top view of the specimen showing different debonding zones.

Specimens 1 and 2 were used for the investigation of lengthwise and widthwise debonding at the centre of the structure, specimen 3 was used for the investigation of widthwise debonding on the side of the structure while specimens 4 and 5 were used for the investigation of patch

debonding. Figure 4 shows the photographic image of the specimen with the location of different debonding zones for lengthwise and widthwise debonding.

3. Results and discussion

3.1 Lengthwise debonding at the centre of the structure

In this measurement, 1.4 mm deep and 1 mm wide debonding was investigated with varying length. First, 20 mm long debonding was created during the application of epoxy and the CFRP plates were placed over it till the epoxy hardened. Similar procedures were followed for debonding lengths 40 mm, 60 mm, 80 mm and 100 mm. Specimens 1 and 2 were inspected in this study. The schematic of the experimental setup and the position of CFRP plates with respect to the debonds is shown in Figure 5.

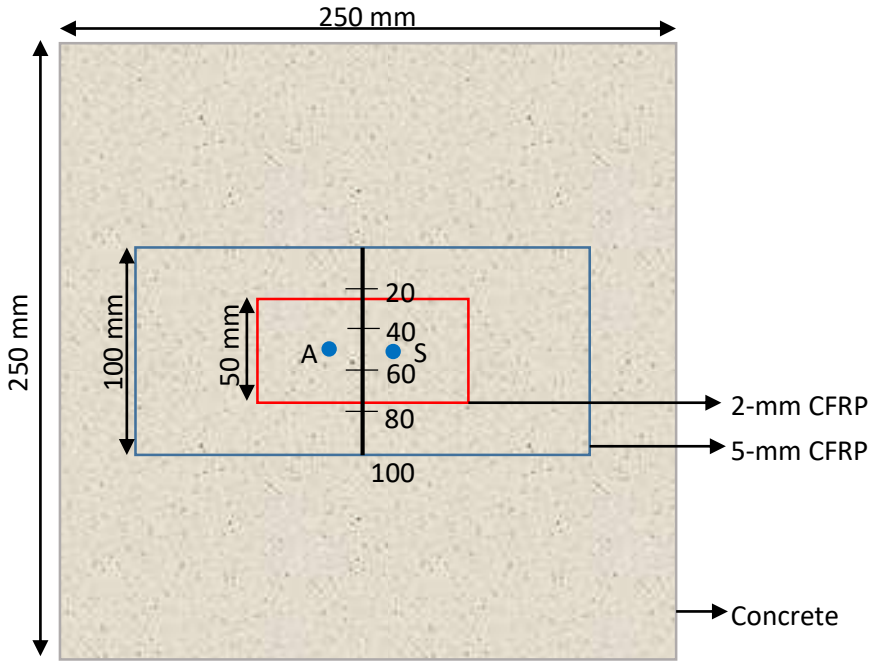

Figure 5. Schematic of experimental setup showing the position of CFRP plates on the concrete block with lengthwise debonding in specimens 1 and 2.

The maximum standard deviation of the reference signal and the signal at debondings with length 20 mm, 40 mm, 60 mm, 80 mm and 100 mm in specimen 1 were determined to be 0.005, 0.008, 0.002, 0.004, 0.004 and 0.004, respectively. Similarly, the standard deviation of the reference signal and the signal at debondings with length 20 mm, 40 mm, 60 mm, 80 mm and 100 mm were 0.018, 0.013, 0.007, 0.017, 0.011 and 0.019, respectively in specimen 2. The low values of standard deviation show the good repeatability rate of the measurement. Next, the

correlation coefficient [30] was determined between the average reference signal and the average signal at each debonding for both specimens using equation 1.

$$Correlation\ coefficient = \frac{n\sum xy-(\sum x)(\sum y)}{\sqrt{n(\sum x^2)-(\sum x)^2}-\sqrt{n(\sum y^2)-(\sum y)^2}} \qquad (1)$$

where n is the number of data, x is the reference signal, and y is the signal with debondings at each time interval.

The higher correlation coefficient value means more similarity between the signal and hence less damage. Therefore, ‘‘1 – cc (correlation coefficient)’’ is used instead of correlation coefficient as a first damage index so that the damage index would increase with the severity of the damage. The “1 – cc” plot for increasing debonding length in specimen 1 and specimen 2 is shown in Figures 6(a) and 6(b), respectively. It can be seen from the plots that the “1 – cc” index increased with increasing debonding length which shows that the dissimilarity between the reference signal and signal with debonding increased. Further, linear fitting was carried out. The coefficient of determination (R^2) for specimen 1 was determined to be 0.93, and for specimen 2, R^2 was determined to be 0.91. These values implied that further debonding could be predicted by extrapolating this fitted curve.

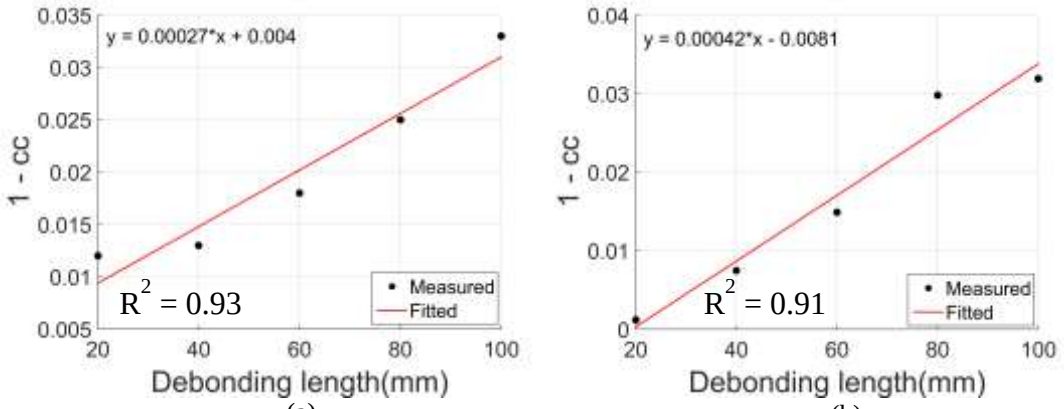

Figure 6. 1 - correlation coefficient with fitted curves at different debonding lengths in (a) specimen 1 and (b) specimen 2.

The second damage index is P2P amplitude. To get P2P amplitude, the resultant signal was obtained at each lengthwise debonding by subtracting the average signal at these debondings against the average reference signal. The P2P amplitude of this resultant signal was plotted,

and linear fitting was applied. The P2P amplitude plot for both specimens is shown in Figures 7(a) and 7(b), respectively. Similar to the previous index, the P2P amplitude increased with the increasing debond size. From linear fitting, R^2 was determined to be 0.91 in specimen 1 and 0.96 in specimen 2.

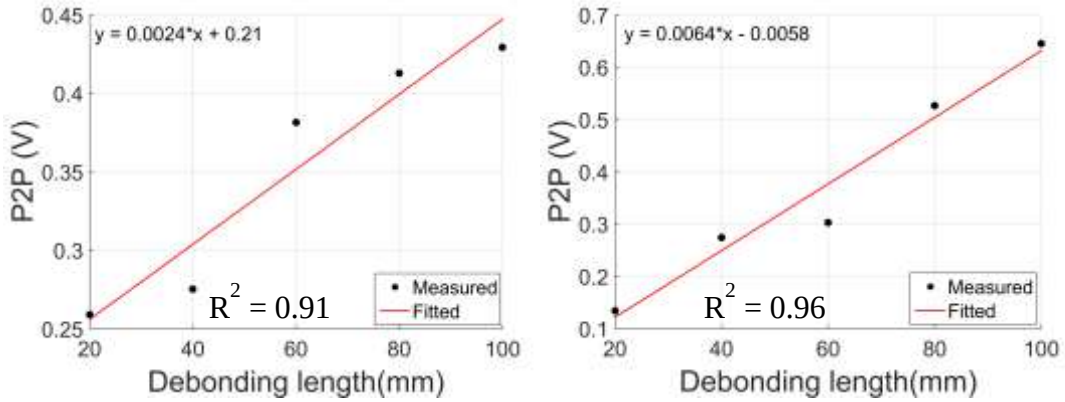

(a) (b)

Figure 7. Change in P2P voltage of the resultant signal with fitted curves at different debonding lengths in (a) specimen 1 and (b) specimen 2.

The next damage index is the root mean square deviation (RMSD) [31]. RMSD is given by equation 2.

$$RMSD(\%) = \sqrt{\frac{\sum_{i=1}^{N}(z(i)-z_0(i))^2}{\sum_{i=1}^{N}(z(i))^2}} \times 100 \qquad (2)$$

where $z(i)$ is the reference signal and $z_0(i)$ is the signal with debondings at each time interval.

Figures 8(a) and 8(b) shows the RMSD at different debonding lengths for specimen 1 and specimen 2, respectively. For specimen 1, the RMSD values increased from 0.32 to 0.49 for debonding length ranging from 20 mm to 100 mm. For specimen 2, the RMSD values increased from 0.11 to 0.49 for the same range of the debonding length. The results show that increasing debonding length increased the RMSD value and followed the same trend as the previous damage indices. It was also noted that the change in RMSD index between 20 mm and 80 mm debonding is higher in specimen 2 with thinner CFRP plate.

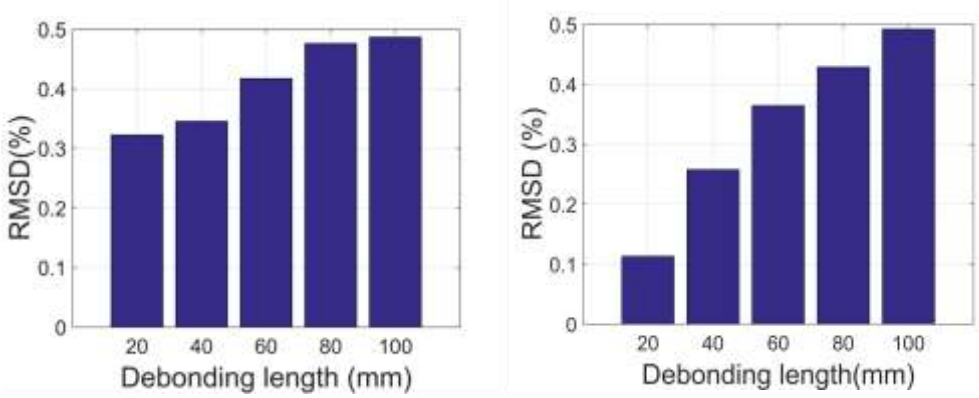

Figure 8. RMSD at different debonding lengths in (a) specimen 1 and (b) specimen 2.

3.2 Widthwise debonding at the centre of the specimen

In this measurement, 1.4 mm deep and 100 mm long debond was investigated with varying width. The debondings of width 2 mm, 4 mm, 6 mm and 8 mm were introduced to the structure near the centre. The measurements were performed in specimen 1 and specimen 2. The schematic of the experimental setup and the position of CFRP plates with respect to the debondings is shown in Figure 9.

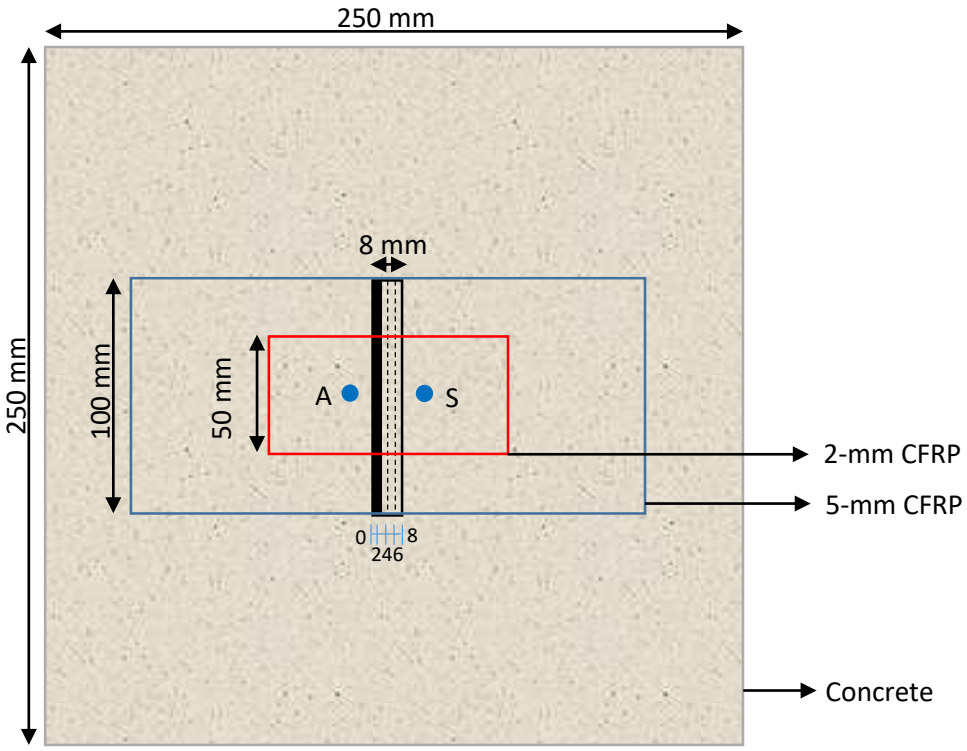

Figure 9. Schematic of experimental setup showing the position of CFRP plates on the concrete block with widthwise debonding in specimens 1 and 2.

The maximum standard deviation of the reference signal and the signal at debondings with width 2 mm, 4 mm, 6 mm and 8 mm in specimen 1 were determined to be 0.005, 0.018, 0.010, 0.006 and 0.076, respectively. Similarly, the standard deviation of the reference signal and the signal at debondings with length 2 mm, 4 mm, 6mm and 8 mm were determined to be 0.018, 0.019, 0.013, 0.018 and 0.027, respectively in specimen 2. Next, the correlation coefficient was determined between the average reference signal and the average signal at each debonding width for both specimens and "1-cc" index was plotted. The "1-cc" plot for increasing debonding width in specimen 1 and specimen 2 is shown in Figures 10(a) and 10(b), respectively. "1-cc" index increased with increasing debonding width in both specimens. Further, linear fitting was carried out. The R^2 values for both specimen 1 and specimen 2 were determined to be 0.98.

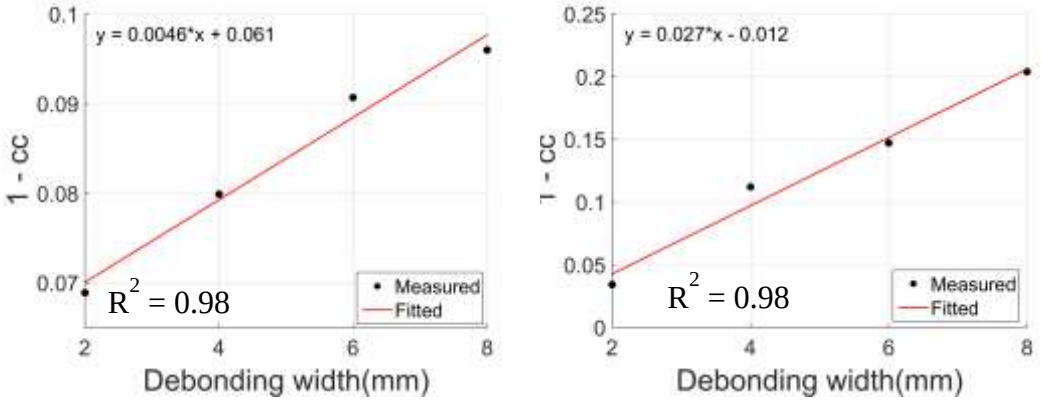

(a) (b)

Figure 10. 1 - correlation coefficient with fitted curves at different debonding widths in (a) specimen 1 and (b) specimen 2.

Next, the P2P amplitude of the resultant signal was plotted, and linear fitting was applied. The P2P amplitude plot for both specimens is shown in Figures 11(a) and 11(b), respectively. The P2P amplitude increased with the increasing gap. From linear fitting, R^2 was determined to be 0.83 in specimen 1 and 0.93 in specimen 2. The low R^2 value in specimen 1 is mainly because of an atypical value obtained for 8 mm width debonding which can be attributed to a measurement error which is also highlighted by higher standard deviation value compared to other debonding measurements.

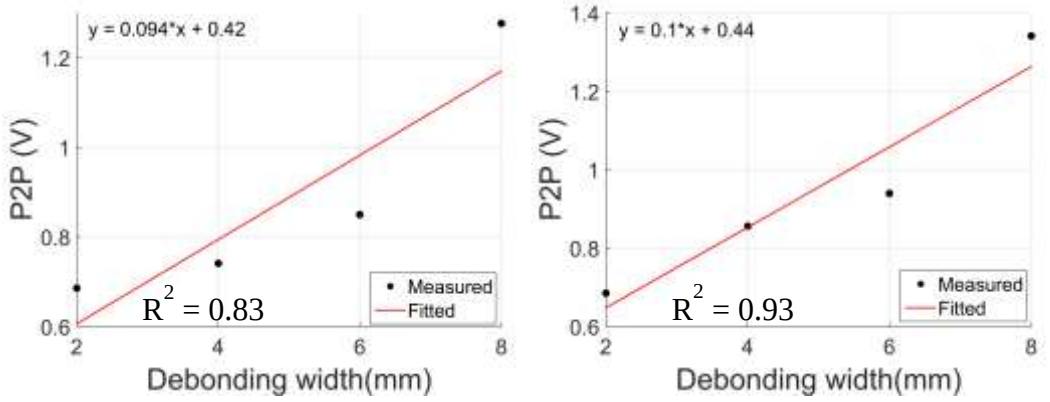

Figure 11. Change in P2P voltage of the resultant signal with fitted curves at different debonding widths in (a) 5-mm CFRP and (b) 2-mm CFRP.

The RMSD at different debonding widths were plotted as shown in Figure 12. The RMSD values increased from 0.78 to 1.54 for debonding width ranging from 2 mm till 8 mm in specimen 1. The measurement error described previously is the reason for irregularly large RMSD value at 8 mm width. Similarly, the RMSD values increased from 0.58 to 1.33 in specimen 2. The RMSD values accurately correlated with the increase in damage (i.e. the width of debonding).

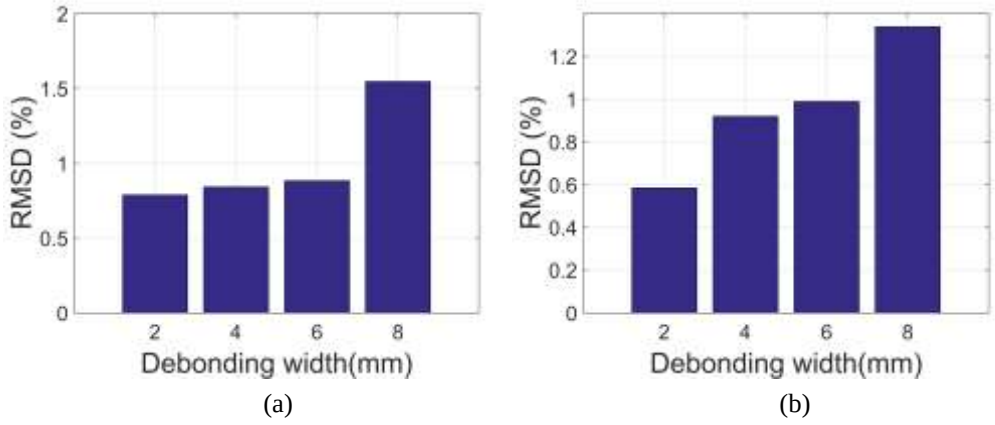

Figure 12. RMSD at different debonding widths in (a) specimen 1 and (b) specimen 2.

Increasing the debonding size both lengthwise and widthwise in the centre of the specimen showed a linear change in all the damage indices (correlation coefficient, change in P2P and RMSD). The results indicated that as the size of debonding increased, the sensitivity of

detecting the debonding also increased. The debonding of size as small as 10 mm x 1 mm x 1.4 mm were detected accurately.

3.3 Widthwise debonding in the side of the specimen

The lengthwise and widthwise debonding were successfully detected in the previous section. However, the debondings were produced in the centre of the specimen and the debonding region lied between the actuator and the sensor. The debonding directly obstructed the path of the generated sine burst signal from the actuator to sensor resulting in accurate detection. However, in a real-life scenario, the origin of debonding would be unknown, and there is a need to detect debondings even when they originate in different locations away from the piezoelectric transducers. For this reason, measurements with widthwise debondings were made on the side of the specimen 3. The schematic of the experimental setup and the position of CFRP plates with respect to the debondings is shown in Figure 13 while the photographic image is shown in Figure 14.

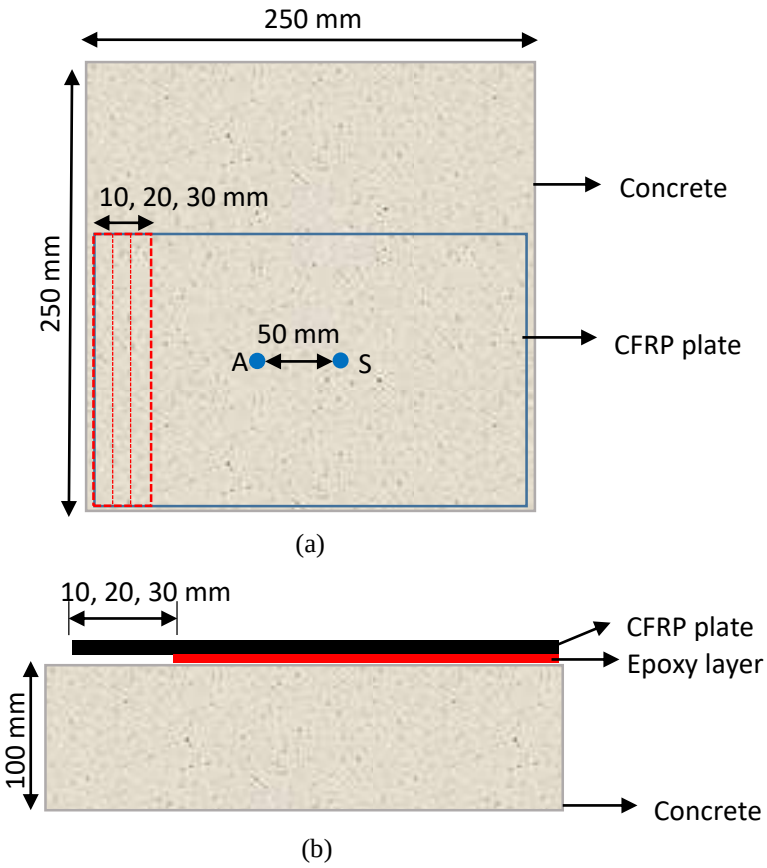

Figure 13. Schematic of experimental setup showing the position of CFRP plate on the concrete block with widthwise debonding in specimen 3: (a) top view and (b) side view.

A reference data was taken at perfect bonding, and different debonding condition was obtained at the left end of the CFRP and concrete bond (ref. Figure 14). The debonding with a depth of 2 mm and a length of 235 mm at different widths were investigated. The three widths – 10 mm, 20 mm and 30 mm were made to simulate three debonding conditions.

(a) (b)

Figure 14. Photographic image of specimen 3 and the experimental setup for widthwise side debonding: (a) top view and (b) side view.

The maximum standard deviation of the reference signal and the signal at debondings with width 10 mm, 20 mm and 30 mm in specimen 3 were determined to be 0.019, 0.007, 0.011 and 0.006, respectively. The "1-cc" index was plotted for different debonding widths as shown in Figure 15(a). Similarly, another index "change in P2P" was plotted for different debonding widths as shown in Figure 15(b). The R^2 values for the fitted curve of the "1-cc" index were determined to be 0.97 and of "change in P2P" index was determined to be 0.99. Again, the high R^2 value shows that these indices are changing linearly with changing debonding value and thus could be used to predict the extent of debonding.

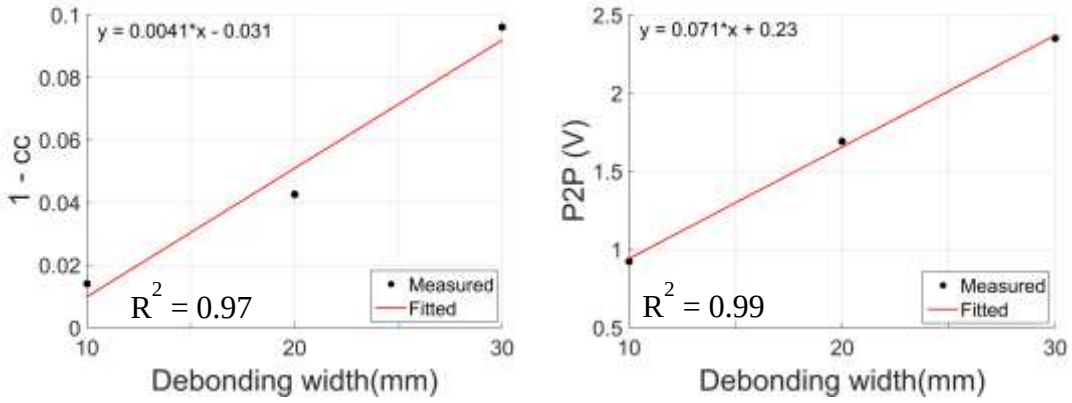

(a) (b)

Figure 15. Statistical indexes with fitted curves at different debonding widths: (a) 1 – correlation coefficient and (b) change in P2P voltage of the resultant signal.

The next damage index, RMSD at different debond widths for specimen was plotted as shown in Figure 16. The RMSD values for debonding widths 10 mm, 20 mm and 30 mm were determined to be 0.253, 0.450 and 0.640, respectively. As expected, RMSD values were increasing linearly with increasing debond size.

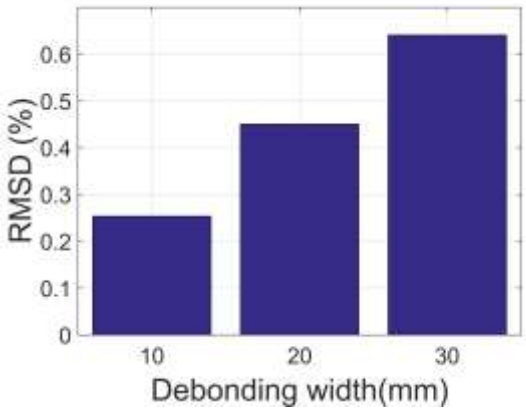

Figure 16. RMSD at different debonding widths in specimen 3.

3.4 Patch debonding at the centre of the specimen

After accurate detection of lengthwise and widthwise debonding, different patch debondings were investigated at the centre of the specimen. This investigation was performed to understand the effect of smaller debonding sizes on the damage indices. First, three different circular debonding patches with diameter 15 mm, 25 mm and 35 mm were made. These patches were used to simulate debonding without sharp edges. Next, three different square debonding patches with sides 17 mm, 28 mm and 37 mm were made. These patches were used to simulate

debonding with sharp edges. The schematic of experimental setup with the position of CFRPs on the concrete and debonding location is shown in Figure 17. Specimen 4 and 5 were used for this investigation.

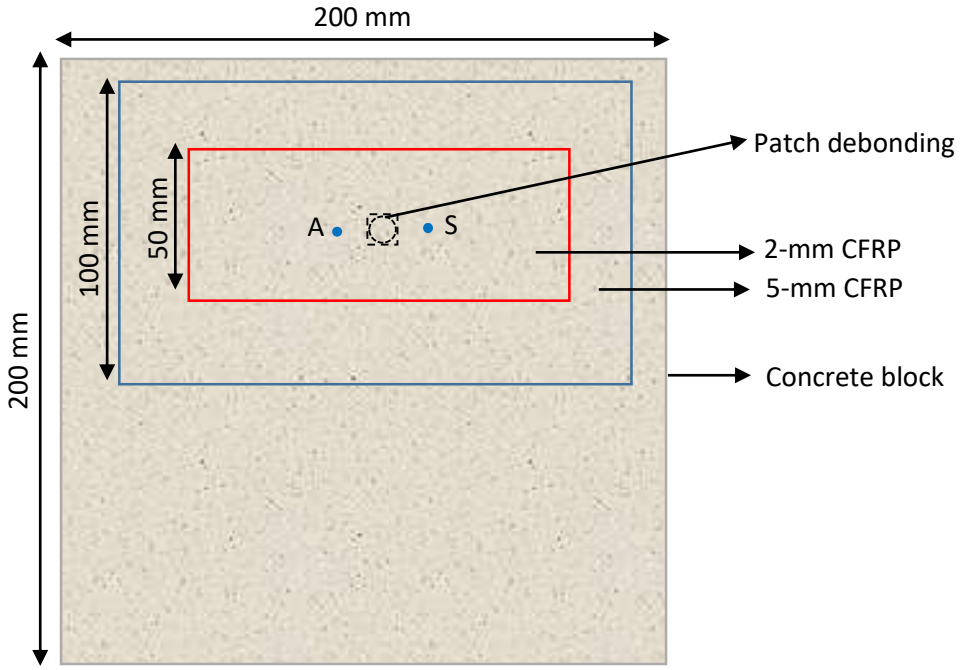

Figure 17. Schematic of experimental setup showing the position of CFRP plates on the concrete block with patch debonding in specimen 4 and 5.

Multiple measurements were taken with a perfectly bonded structure and with different sized circular and square patches. For specimen 4, the maximum standard deviation of the reference signal and circular patch debonding of diameter 14 mm, 25 mm and 35 mm were determined to be 0.060, 0.088, 0.108 and 0.035, respectively. Similarly, the maximum standard deviation of the reference signal and square patch debonding with sides 17 mm, 28 mm and 37 mm were determined to be 0.060, 0.168, 0.031 and 0.034, respectively. For specimen 5, the maximum standard deviation of the reference signal and circular patch debond of diameter 14 mm, 25 mm and 35 mm were determined to be 0.025, 0.004, 0.013 and 0.035, respectively. Similarly, the maximum standard deviation of the reference signal and square patch debond with sides 17 mm, 28 mm and 37 mm were determined to be 0.025, 0.008, 0.008 and 0.036, respectively.

Figure 18 shows ‘‘1 – cc” index for different circular and square patch debondings with increasing debonding values. Similar to the previous results, there was a clear indication of a change in damage index with increasing damage severity. Further, square debondings showed a more significant change in the indices compared to the circular debondings on both these

specimens. This difference is mainly due to the sharp edges of square debondings due to which there was a significant change in the reflected signal compared to the reference signal. Also, the change in the signal between square and circular debondings are higher in the specimen 4 (ref. Figure 18(a)) compared to the specimen 5 (ref. Figure 18(b)). This might be due to the thinner CFRP plate used in specimen 4 which led to higher sensitivity.

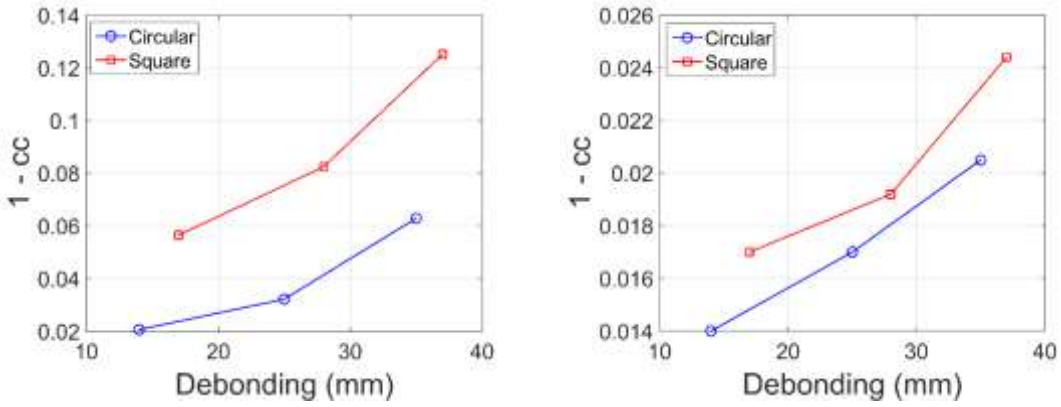

(a) (b)

Figure 18. 1 - Correlation coefficient at different patch debondings in (a) specimen 4 and (b) specimen 5.

Next, change in P2P voltage was plotted with respect to change in debonding values of circular and square patches as shown in Figure 19. Similar observations were made with the indices increasing with increasing damage severity.

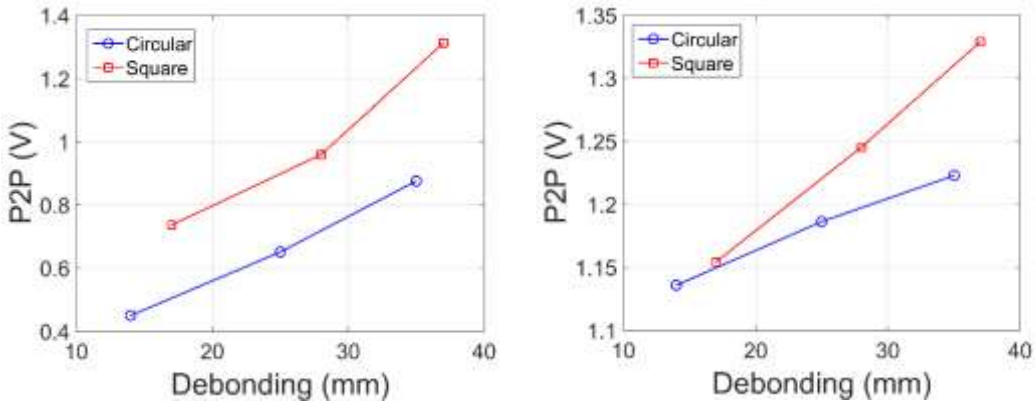

(a) (b)

Figure 19. Change in P2P voltage of the resultant signal at different patch debondings in (a) specimen 4 and (b) specimen 5.

The next damage index, RMSD at different circular and square patch debondings were plotted as shown in Figure 20. The RMSD values for circular debondings in specimen 4 with diameter 14 mm, 25 mm and 35 mm were determined to be 0.475, 0.632 and 0.750, respectively. Similarly, the RMSD values for square debondings with sides 17 mm, 28 mm and 37 mm were determined to be 0.775, 0.846 and 1.116, respectively. In specimen 5, the RMSD values for circular debondings with a diameter of 14 mm, 25 mm and 35 mm were determined to be 0.472, 0.488 and 0.520 respectively. Similarly, for square debondings with sides 17 mm, 28 mm and 37 mm, the RMSD values were determined to be 0.479, 0.494 and 0.537, respectively. As the other damages indices suggested, RMSD values also increased with increasing debonding size. Further, the sensitivity to different types of damage in specimen 4 with thinner CFRP plate was higher than in specimen 5 with thicker CFRP plate.

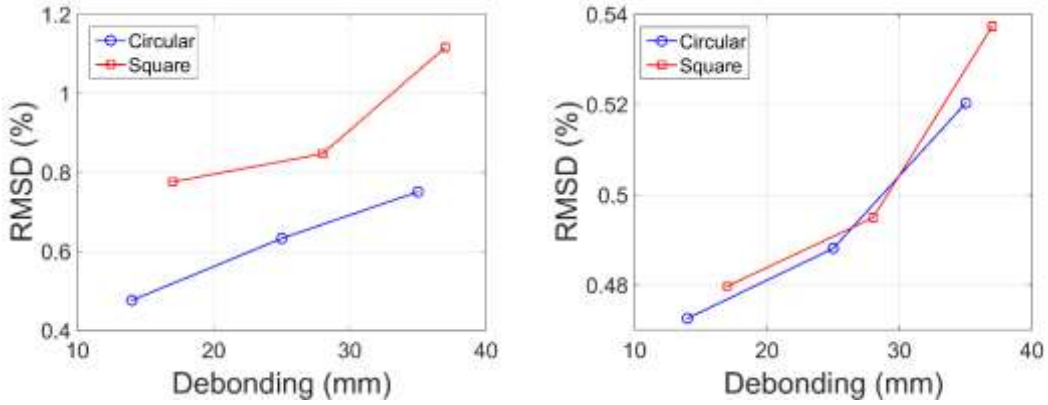

(a) (b)

Figure 20. RMSD values at different patch debondings in (a) specimen 4 and (b) specimen 5.

The above results show that the size of debonding increased all three damage indices and the change in the values of these damage indices correlated with the extent of damages. This correlation shows that the proposed technique is also able to detect patch debonding besides the lengthwise and widthwise debonding described in the previous section.

Conclusion

In this study, a single actuator and a single sensor attached on the surface of the CFRP was used to investigate debonding in a CFRP reinforced concrete structure. A lamb wave was generated, and the received signal at a perfectly bonded condition was taken as a reference. This signal was compared with the damage signal at different debonding conditions. For

comparison and quantification, three damage indices: correlation coefficient, change in P2P and RMSD were employed. Different specimens were prepared with different debonding conditions. These debonding conditions were lengthwise, widthwise and patch debonding at different positions with respect to the transducers. The results demonstrated that all of the damage indices correlate with the extent of the damage. Further, the high coefficient of determination values proved that the extent of debonding could be predicted from the linearly fitted curve. The developed technique can be utilised to detect interfacial defects in a variety of composite structures, and the main advantage of the technique over the conventional technique is the usability in an existing structure.

References

[1] Buyukozturk O, Gunes O and Karaca E 2004 Progress on understanding debonding problems in reinforced concrete and steel members strengthened using FRP composites *Construction and Building Materials* **18** 9-19

[2] Teng J, Chen J-F, Smith S T and Lam L 2002 FRP: strengthened RC structures *Frontiers in Physics* 266

[3] Beydokhti E Z and Shariatmadar H 2016 Strengthening and rehabilitation of exterior RC beam–column joints using carbon-FRP jacketing *Materials and Structures* **49** 5067-83

[4] Ozbakkaloglu T and Xie T 2016 Geopolymer concrete-filled FRP tubes: Behavior of circular and square columns under axial compression *Composites Part B: Engineering* **96** 215-30

[5] Ekenel M, Rizzo A, Myers J J and Nanni A 2006 Flexural fatigue behavior of reinforced concrete beams strengthened with FRP fabric and precured laminate systems *Journal of Composites for Construction* **10** 433-42

[6] Firmo J P, Correia J R and França P 2012 Fire behaviour of reinforced concrete beams strengthened with CFRP laminates: Protection systems with insulation of the anchorage zones *Composites Part B: Engineering* **43** 1545-56

[7] Cuomo M, Caponetto R, Presti A L and Ardizzone E 2017 Experimental evaluation of the effect of partial saturation of construction moisture on CFRP-concrete debonding *Composites Part B: Engineering* **127** 70-7

[8] Verstrynge E, Wevers M, Ghiassi B and Lourenço P B 2015 Debonding damage analysis in composite-masonry strengthening systems with polymer-and mortar-based matrix by means of the acoustic emission technique *Smart Materials and Structures* **25** 015009

[9] Kharkovsky S, Ryley A C, Stephen V and Zoughi R 2008 Dual-polarized near-field microwave reflectometer for noninvasive inspection of carbon fiber reinforced polymer-strengthened structures *IEEE Transactions on Instrumentation and Measurement* **57** 168-75

[10] Akuthota B, Hughes D, Zoughi R, Myers J and Nanni A 2004 Near-field microwave detection of disbond in carbon fiber reinforced polymer composites used for strengthening cement-based structures and disbond repair verification *Journal of Materials in Civil Engineering* **16** 540-6

[11] Halabe U B, Vasudevan A, Klinkhachorn P and GangaRao H V 2007 Detection of subsurface defects in fiber reinforced polymer composite bridge decks using digital infrared thermography *Nondestructive Testing and Evaluation* **22** 155-75
[12] Lai W, Lee K, Kou S, Poon C and Tsang W 2012 A study of full-field debond behaviour and durability of CFRP-concrete composite beams by pulsed infrared thermography (IRT) *NDT & E International* **52** 112-21
[13] Degala S, Rizzo P, Ramanathan K and Harries K A 2009 Acoustic emission monitoring of CFRP reinforced concrete slabs *Construction and Building Materials* **23** 2016-26
[14] Qiu Q and Lau D 2016 The Sensitivity of Acoustic-Laser Technique for Detecting the Defects in CFRP-Bonded Concrete Systems *Journal of Nondestructive Evaluation* **35** 1-10
[15] Hsieh C-T, Lin Y and Lin S-K 2017 Impact-echo method for the deterioration evaluation of near-surface mounted CFRP strengthening under outdoor exposure conditions *Materials and Structures* **50** 72
[16] Yu T-Y and Büyüköztürk O 2008 A far-field airborne radar NDT technique for detecting debonding in GFRP–retrofitted concrete structures *NDT & E International* **41** 10-24
[17] Arone M, Cerniglia D and Nigrelli V 2006 Defect characterization in Al welded joints by non-contact Lamb wave technique *Journal of Materials Processing Technology* **176** 95-101
[18] Ng C-T and Veidt M 2009 A Lamb-wave-based technique for damage detection in composite laminates *Smart Materials and Structures* **18** 074006
[19] Mitra M and Gopalakrishnan S 2016 Guided wave based structural health monitoring: A review *Smart Materials and Structures* **25** 053001
[20] Ihn J-B and Chang F-K 2008 Pitch-catch active sensing methods in structural health monitoring for aircraft structures *Structural Health Monitoring* **7** 5-19
[21] Wu F and Chang F-K 2006 Debond detection using embedded piezoelectric elements in reinforced concrete structures-part I: experiment *Structural Health Monitoring* **5** 5-15
[22] Xu B, Chen H and Xia S 2017 Wave propagation simulation and its wavelet package analysis for debonding detection of circular CFST members *Smart Structures and Systems* **19** 181-94
[23] Xu Y and Liu G 2002 A modified electro-mechanical impedance model of piezoelectric actuator-sensors for debonding detection of composite patches *Journal of Intelligent Material Systems and Structures* **13** 389-96
[24] Wang Y, Zhu X, Hao H and Ou J 2009 Guided wave propagation and spectral element method for debonding damage assessment in RC structures *Journal of Sound and Vibration* **324** 751-72
[25] Wang Y and Hao H 2014 Modelling of guided wave propagation with spectral element: application in structural engineering *Applied Mechanics and Materials* **553** 687-92
[26] Park S, Kim J-W, Lee C and Park S-K 2011 Impedance-based wireless debonding condition monitoring of CFRP laminated concrete structures *NDT & E International* **44** 232-8
[27] Giri P and Kharkovsky S 2017 Detection of gap in concrete-metal structures using piezoelectric sensor technique. In: *Instrumentation and Measurement Technology Conference (I2MTC), 2017 IEEE International*: IEEE) pp 1-5
[28] Giri P, Kharkovsky S, Zhu X, Clark S M, Taheri S and Samali B 2018 Characterization of carbon fiber reinforced polymer strengthened concrete and gap detection with a piezoelectric-based sensory technique *Structural Health Monitoring* 1475921718803790

[29] Sika Australia 2014 Sikadur-30 Adhesive for bonding reinforcement. In: *Product Datasheets: Sika D*: Sika Group) pp 1-5
[30] Su Z, Wang X, Chen Z, Ye L and Wang D 2006 A built-in active sensor network for health monitoring of composite structures *Smart Materials and Structures* **15** 1939
[31] Tseng K K and Wang L 2004 Smart piezoelectric transducers for in situ health monitoring of concrete *Smart Materials and Structures* **13** 1017